PALEO-POLE POSITIONS FROM MARTIAN MAGNETIC ANOMALY DATA

James J. Frawley
Herring Bay Geophysics
440 Fairhaven Road
Tracys Landing,MD20779
(301)855-6169
hbgjif@ltpmailx.gsfc.nasa.gov

Patrick T.Taylor
Geodynamics Branch
NASA/Goddard Space Flight Center
Greenbelt,MD
(301)614-5214
Fax (301)614-6522
ptaylor@ltpmail.gsfc.nasa.gov

33 Pages, 7 Figures,2 tables

Running Heading: Martian paleo-poles

contact: James J. Frawley

440 Fairhaven Road

Tracys Landing.MD20754

(301)855-6169

hbgjjf@ltpmailx.gsfc.nasa.gov

Abstract

Magnetic component anomaly maps were made from five mapping cycles of the Mars Global Surveyor's magnetometer data. Our goal was to find and isolate positive and negative anomaly pairs which would indicate magnetization of a single source body. From these anomalies we could compute the direction of the magnetizing vector and subsequently the location of the magnetic pole existing at the time of magnetization. We found nine suitable anomaly pairs and from these we computed paleo-poles that were nearly equally divided between north, south and mid-latitudes. These results suggest that during the existence of the martian main magnetic field it experienced several reversals and excursions.

Key words: Mars, Data Reduction Techniques, Geophysics, Magnetic Fields.

Introduction

As a part of the NASA planetary exploration program the Mars Global Surveyor (MGS) mission was launched on November 7, 1996 to characterize and describe the surface and environment of this planet. It arrived at Mars ten months later. A triaxial

fluxgate magnetometer and electron reflectometer (MAG/ER) were part of the instrument payload (Acuña et. al., 1998). The fluxgate instrument records three mutually orthogonal magnetic field components. It was revealed by the initial magnetic anomaly maps computed from these data that, unlike Earth, Mars lacks a dipole or main magnetic field (Acuña et. al.,1999, Ness et al., 2000, Purucker et al.,2000 and Connerney et al., 2001). However, these early results discovered that there were many high amplitude magnetic anomalies produced by large contrasts in magnetization. By far the majority of these were located in the southern highlands and were uncorrelated with either topography or the large impact basins. Since there was no inducing core magnetic field these anomalies must have been produced by a remanent magnetization process. When rock magnetization is present in the absence of an external field then they have been magnetized by remanence. Several different processes can produce this effect (*e.g.*, McElhinny and McFadde, 2000). These remanently magnetized rock record or remember the initial magnetizing field even after the field has been removed. Previously Curtis and Ness (1988), Lewelling and Spohn (1997) and Ness et al., (1999) had proposed that this process might be occuring on Mars. There have been several previous interpretations, on a planetary scale, of the geological significance of these crustal anomalies (Connerney et al, 1999 and 2001; Arkani-Hamed, 2001 and 2002; and Purucker et al., 2000). For example,Connerney et al. (1999) interpreted these anomalies as indicating an earlier period of plate tectonics. This hypothesis has been discussed by others (Harrison, 2000, Connerney et al., 2000 and Nimmo, 2000). In our present study, however, we select isolated and distinct positive and negative anomaly pairs that are characterized by the magnetization of a single source body by a dipole field. We compute the magnetization vector and subsequently determine the location of the magnetizing pole. Essentially we are deriving a virtual geomagnetic pole as described by Irving (1964). Similar studies

have been done by Hood and Zakharian (2001) and Arkani-Hamed (2001 and 2002). We selected nine distinct positive and negative anomaly pairs from the martian crustal anomaly field. When comparing satellite altitude magnetic anomaly data from the Earth with Mars we find that there are more isolated anomalies in the martian field than on Earth (cf., Langel and Hinze, 1998 and Connerney et al, 1999) since the latter are often formed by overlapping sources that produce indistinct anomalies. Previously we computed a virtual geomagnetic pole for the large and isolated Kursk magnetic anomaly of Russia (Taylor and Frawley, 1987). However, in this report we describe how we selected isolated magnetic anomalies and how they were used to derive paleo-pole positions on Mars

Data Processing

Data from the magnetometer/electron reflectometer (MAG/ER) experiment aboard the MGS (Acuña et al., 1998) was obtained from the Institute of Geophysics and Planetary Physics, Planetary Data System at the University of California, Los Angeles for the periods covering the aero-braking phase, Science Phasing Orbits 1 and 2 and the mapping mission from March, 1999 to August, 1999. Only the mapping phase data, approximately five mapping cycles (~28 days/cycle), were used in this study. These data were contained on twenty-four CD-ROMs and included processed orbit information as well as the Magnetometer and Electron Reflectometer Experiment results. In addition to MAG/ER observations, magnetic compensation fields and spacecraft currents for each observation were recorded. The magnetic compensation fields included both static and dynamic terms for each axis. The rms field of each axis was also recorded to aid in the detection of external field and instrument noise.

Initially, global maps of the martian crustal magnetic field were produced using night-side passes acquired from the mapping phase data collected from 3/8/99 to 5/4/99. The night-side passes were used to avoid the martian magnetosphere produced by solar radiation. Data were selected between 87° North and 87° South. Each magnetic component (X, Y and Z, positive in the North ,East and Vertical (downward) directions respectively) was de-trended with a second-order-Fourier series, and the selected passes were screened manually for external field effects. After a relatively clean set of passes were obtained, they were binned in spherical coordinates at a one-degree grid interval (*i.e.*, approximately 59 km at the equator). Global maps for the three components are shown in Fig. 1. Visual inspection of these maps at once showed two things: a) the martian crustal magnetic field, like the topography, is dichotomous; and b) a number of isolated positive and negative anomalies could be modeled as being produced from the magnetization of a single isolated body. These aspects of the martian magnetic anomaly field have been noted by other investigators (Acuña et al., (1999), Arkani-Ahmed (2001 and 2002), Hood and Zakharian (2001), Purucker et al.(2000)) and others. The dichotomous crustal field does not correlate with the topography except only in the most general sense. That is, the highly magnetized crust occurs in the southern hemisphere and is generally centered longitudinally on the southern-cratered highlands. Using these global maps, a number of areas were selected for more detailed analysis. These were all regions where there were isolated anomalies, with the exception of the region of high magnetization (RHM), which was analyzed separately. Figure 2 shows the locations of the seven study areas, each of which was in turn sub-divided into regions where the individual isolated anomalies occurred.

gure 1 here

Production of final contour maps for selected regions of the planet Mars took place in eight steps:

gure 2 here

1) Extract data selected for each chosen area from the sixteen mapping phase CD ROMs , rotate into planetary coordinates and concatenate.

2) Sort and number tracks as ascending or descending and plot on map projection.

3) De-trend tracks with a first-order polynomial.

4) Grid descending tracks at 40 km interval using minimum curvature/Akima interpolator algorithms.

5) Sort descending tracks used to make initial grid by longitude and plot F (scalar field), X, Y and Z in groups of five. Each group of five was then screened manually for external noise, *i.e.*, non-crustal fields.

6) Generate a new selection of descending orbits excluding bad or noisy tracks.

7) Re-grid tracks using culled data set.

8) Low-pass filter gridded data using cutoff wavelengths of 400 to 160 km.

This process was done separately for the each of the total field and X, Y and Z components. After viewing profiles from several full orbits it was decided to use only the more noise free descending or night time passes in making the magnetic maps. This is because the MGS is in a sun-synchronous orbit, crossing the equator at 2 pm local on the ascending pass and 2 am local on the descending pass. Thus, the descending passes suffered less from external fields and gave a better representation of the crustal fields (Ness et al., 2000). A first order polynomial was used to de-trend each track after trying polynomials of orders 0 through 4. The first order polynomial seemed to give the best match of adjacent profiles and did not introduce any artificial frequencies into the data. Figure 3 shows a sample of profiles of adjacent tracks .

Figure 3 here

The altitude range of the passes used in making the global map, consisting only of nightside passes, varied from about 356 to 423 km, with the mean altitude at about 391 km. These orbits describe a relatively smooth surface, with the high altitudes being up near the North pole and the low altitudes near the South. For the 60x60 degree areas the altitude range was about 370 to 390 km., *i.e.*, an altitude range of ±10 km, which is about what we previously used as an altitude window in processing MAGSAT data. The major difference being that, with the MAGSAT data, we often had orbits of max-min altitude adjacent to each other, whereas with MAG/ER, the altitudes are fairly constant along bands of latitude, tilting gradually upwards from South to North (*i.e.*, describing a smooth surface).

There were generally about 300 tracks in each 60 x 60 degree area. After eliminating tracks with high noise/external field levels, there were usually about 250 usable tracks remaining. Figure 4 is an example of the data from one of our study areas, number 2, and shows all the tracks used in making the final smoothed contour map.

Crustal Anomaly Maps

Using the processing procedures previously described, magnetic anomaly maps were generated for seven 60 x 60 degree regions. All the areas except one covered the latitude band 50°S-10°N. The extent of areas 1-7 is listed in Table 1 and shown in Fig. 2.

ıble 1 Test Area Limits

Figure 4 here

Final contours for the X, Y and Z components for each of the areas are shown in Fig. 6 (a-g). All the isolated anomalies displayed the classic morphologies of an isolated source. The relative positions of the highs and lows for each component gave an indication of the direction of magnetization, and the spacing between the highs and lows an indication of depth to source (Blakely, 1995).

All of our magnetic anomaly locations are in the martian highlands and all but two are located in the southern hemisphere (Fig. 2). One isolated anomaly occurs in Area 1 (Table 1 and Fig. 2) on the southern edge of Claritis Rupes , the western border of Syria Planum, however there is no significant correlation between this anomaly and any distinct physiographic feature. Area 2 partially overlaps the western most section of Area 1. There were three isolated anomaly pairs selected from this region. The eastern most of these anomalies lies at the extreme base of Arsia Mons on Daedalia Planum with the vertical component coincident with the crater Amazonis Sulci, however, this crater is small and may or may not be related to the anomaly. The other two isolated anomalies we selected from this area are between the craters Marca and Burton and Comas Sola and Bernard. However, the western half of Area 2 is heavily cratered, and any anomaly in this area would lie on or near a crater. It must be mentioned again that our criterion for anomaly selection is based on choosing isolated anomalies with developed single source features, that is, a distinct or recognizable positive and negative doublet anomaly pair and not on the largest amplitude fields. Three isolated anomalies were analyzed from Area 3. This region is dominated by the Valles Marinaris and the northern half of Argyre Planitia, however, one anomaly lies to the north and the others further to the south of this feature. The northernmost anomaly is on the Ophir Planum, just west of the Ganges Chasm, on the southwestern boundary of the larger Xanthe Terra. With one between the Noachis Terra and Bosporus Planum near the crater Bunge. The southernmost anomaly lies to the southwest on the Bosporus Planum, neither of these are correlated with distinct topographic features. The last two selected anomalies are from Area 7 , one near Ares Valles on Arabia Terra and the other on the southern border of Arcadia Planitia.

Analysis

The most striking features to be seen with the generation of the first component maps were the existence of well defined, isolated magnetic sources. These showed the classic distribution of maxima and minima in each component indicative of a single source with a constant direction of magnetization. Since at present Mars has no discernible core field, the formation of these sources are the result of remanence, that is, magnetization occurred in the past when Mars had a main or core field similar to the present day of the Earth (Zatman et al., 2001). Accordingly, each individual area map was examined for isolated magnetic sources and each was marked for further analysis. Other areas were not used either because they did not have any good single source anomalies or because, as in area 6, the field was much more complex. Several methods were used to derive a direction of magnetization. One of the two inverse methods employed was Parker's determination from X, Y and Z components (Parker et al., 1987), originally developed to estimate the magnetization of seamounts (many of which are often text-book examples of isolated anomalies). This technique was found to be far too sensitive to position and size of the data grid to be of use. The other inverse method utilized the application of moments of the components for determining magnetization directions (Helbig, 1963). This proved to be less satisfactory than the first in terms of variability and sensitivity to position and areal extent of the measured data. Even though it had been used successfully in the past to determine direction of magnetization from Magsat data over the Kursk Magnetic Anomaly, Russia (Taylor and Frawley, 1987) it did not work well with the martian anomalies. Finally, fitting a simple dipole or prism source was determined to give the best result in the limiting case.

We used a two stage procedure for determining the direction and intensity of the dipole magnetization vector. In the first, forward modeling was used to estimate the position and magnetization of the dipole source .Adjustments were made to these parameters until the field of the model matched the measured field as closely as possible. The criteria used in matching the fields were the amplitudes and separation of the extrema of the anomaly in each of the X,Y and Z components. This was strictly a trial and error process, but it was usually possible to converge on a reasonable approximation after several iterations. In the second stage, generalized linear least squares was used to obtain an inversion to the magnetization vector. In order to minimize the effect of noise and contamination from near by anomalies, the points selected for input to the inverse program were those that fell within the lowest (absolute value) least distorted (subjective judgment) closed contour around the extrema of the anomaly in each component. Figures 5A, B and C show the points used for anomaly #2. However, because the direction of magnetization computed by the inverse program is very sensitive to the horizontal placement of the dipole - it is less sensitive to the vertical position, at least for satellite measurements - a second iterative procedure was used to determine the optimal position of the dipole source. Starting with the position obtained from the first stage of our procedure, a 400 x 400 km grid, centered on the initial x, y estimate of the dipole position, was superimposed on the anomaly. The spacing of this grid was 40 km, the same as that of the measured data grid. At each point of this grid, the inverse solution

Figure 5 here

was computed, and the rms fit to the input data computed and recorded The resulting 10x10 array of rms values was then contoured to reveal the position at which the rms fit was a minimum. This minimum rms position was used in the final direction of magnetization solution. Figure 5D shows the rms contours for anomaly #2 and the results for all nine models are summarized in Table 2.

This procedure worked well for all but three of the anomalies: numbers 1, 3 and 4. In the case of number 1, there may have been some noise contamination because it was a low amplitude anomaly. For this instance, an initial direction of magnetization was computed using the ratios of the extrema in the X and Y components. The horizontal position of the source was then determined by visually aligning the contours with the measured field. Finally, using this position, an inversion was done to the measured field values.

A closer examination of anomalies 3 & 4 revealed that, although it was possible to match the separation of the extrema in each component by placing the dipole at a greater depth, the depths were so great that the gradients of the resulting model field were much shallower than those of the measured field. To remedy this, the source body would have to be positioned nearer to the planets surface, with some of the spacing of the extrema attributable to the lateral extent of the body. Accordingly, we replaced the dipole sources with polygonal prisms and, using the equations derived by Plouff(1976), repeated the point dipole procedure, described above, using prisms as sources. This resulted in a much improved rms fit of model field to measured field for anomaly 3. Both prisms were 20 km thick with their upper surface at the planets surface. They can be seen in plan view in Figure 6b. It should also be noted that there is some overlap in the X component of these two anomalies. Least squares solutions for the two prisms, both separate and simultaneous, yielded magnetization directions that differed by only a few degrees, suggesting that the overlap did not have a significant effect on the results. Anomalies 4, was further contaminated by a smaller anomaly in the Northeast corner of the area, particularly in the Y component, making its results least reliable.

The depths given for each dipole represent the maximum depth possible for a single source to produce the observed anomaly. And the magnetization is likewise the

maximum. For those depths below the Curie isotherm - estimates of which range from 30 km (Acuña,1999) to as deep as 200 km(Leweling & Spohn,1997) - the depth to the source of the anomaly must lie somewhere above the Curie isotherm in the crust. In some cases, the fields of the point dipole source at depth and a laterally extended, thicker body in the crust can mimic each other exactly. (see, *e.g.*, Section 10, Perspectivity in McMillan,1958). A second issue with depth concerns the resolving power of our method. It is difficult to say at this time how accurately depth can be determined by these methods, but tests with forward modeling suggest that it as about the same as the grid spacing of the data. For example, the distance between the maxima and minima of a point dipole field at satellite altitude will typically increase by one grid interval as the source is moved from the surface to a depth of 40 km. So it is likely that our depth estimates are only good the nearest 40 km; telling us only that the source is in the crust - which is intuitive. However, since the objective of our study is not depth to source, but rather direction of magnetization, we can use this information to estimate the accuracy of our direction calculations. Taking anomaly #2 as an example, we note that placing the dipole at the surface gives a dip of -48.8 and a declination of 4.7, whereas placing it at a depth of 40 km gives a dip of -47.6 and a declination of 3.7, being a difference of about .2 degrees in dip and 1 degree in declination. Thus, the uncertainty in our depth estimation should not have an appreciable effect on our direction of magnetization calculations.

Figure 6 here

After computing the components of the magnetization vector for all nine of our test cases, paleo-pole positions were computed using the basic equations of Butler (1995). These results are included in table 2. Contours of the model fields are shown in Figure 6, plotted directly below the associated measured field contours. Paleo-pole locations are shown in Figure 7.

***Table 2** Dipole odels and paleo-poles*

igure 7 here

Discussion and Conclusion

Several crustal magnetic anomalies have been defined from the MGS MAG/ER data. Paleo-poles computed from these suggest that Mars original magnetic field was at times reversed similar to that of the Earth's. The fact that the declinations of some of the anomalies examined were near zero or 180 degrees indicates that at the time their remenant magnetization was acquired the direction of the martian main dipole field must have been close to the planets' present day axis of rotation. It is not possible at this point to determine when the martian main field disappeared, nor how long it was in existence.

Hood and Zakharian (2001) conducted a similar study on two isolated magnetic anomalies in the martian northern polar region (83° N, 32° E and 65° N, 27° E). They found that the pole positions for these anomalies were situated in an area north of Olympus Mons (50° N, 135° W). Likewise, Arkani-Hamed (2001) computed pole positions for ten small isolated magnetic anomalies in both hemispheres and ranging from 65° N to 27° S latitude. He found that seven of the ten computed poles were distributed within thirty degrees of the point at 25° N latitude, 230° E longitude. Two of our anomalies are located near those studied by Arkani-Hamed (2001); our numbers 2 and 8 correspond with M7 and M10 of Arkani-Hamed (2001) respectively. The results differ significantly (our 2 and M7-paleo-latitude: 70°N versus 35°S and paleo-longitude: 26°E versus 40°E and for 8 and M10 (paleo-latitude: 89°S versus 4°N and paleo-longitude 143°E versus 168°E). Arkani-Hamed(2001) fitted a magnetization vector to a vertical prism with an elliptical cross section whose top was the martian surface while we fitted a vector dipole to the anomaly field itself; similar to the procedure practiced in determining the paleo-pole from seamount data (*e.g.*, Mayhew, 1986). Some of these discrepencies may be accounted for by the different techniques used to isolate the anomalies. However, in the case of the second example, the discrepancy can be explained by what part of the

field is considered as arising from a single source. In our case we considered the high-low pair in the Z component, for example, to be generated by a single horizontally polarized source, whereas Arkani-Hamed's model assumes the Z component is a single high, resulting in a vertically polarized source (implying that the source of the adjacent low is radially polarized in the reverse direction). In the first case it should be noted that the two directions of magnetization are simialr in dip (48° South vs 66° South) but approximately 180° out in declination(4° vs 172° West). Plots of the potential and component fields produced by sources with these two magnetizations show that they are similar in the main features.

Interpretations of satellite altitude anomalies on the Earth are greatly aided by the large amount of geologic, ground-based geophysical and tectonic data (see, Langel and Hinze, 1998). This geologic information is used to define and constrain the interpretations of the magnetic anomalies at satellite altitude, unfortunately, a similar set of data are not available for Mars. In order to begin to make geologically reasonable interpretations we should, at least, know the thickness and structure of the crust and have a representative planetary sampling of the petromagnetic and paleomagnetic properties of the crust; until these data are available we will have divergent views for the interpretation of the magnetic field of Mars.

Acknowledgments

This work was done under NASA Headquarters Grant Number NAG5-9832.

We wish to thank the Planetary Data Center at IGPP of the University of California, Los Angeles for supplying these data.

REFERENCES

Acuña, M. H. and others 1998. Magnetic Field and Plasma Observations at Mars: Initial Results of the Mars Global Survey Mission. Science ***279,*** *1676-1680.*

Acuña, M. H. and others 1999. Global Distribution of Crustal Magnetization Discovered by the Mars Global Survey MAG/ER Experimetn. Science ***284,*** *790-793.*

Arkani-Hamed, J. 2002. Magnetization of the Martian crust. Journal of Geophysical Research ***107,*** *8-1-8-10.*

Arkani-Hamed, J.2001. Paleomagnetic Pole Positions and Pole Reversals of Mars. Geophysical Research Letters ***28,*** *3409-3412.*

Blakeley, R.J. 1995. Potential Theory in Gravity & Magnetic Applications, Cambridge University Press, Cambridge.

Butler, R.F. 1995. Paleomagnetism, Blackwell Scientific Publications, Boston, 319 p.

Connerney, J.E. and other 2001. The Global Magnetic Field of Mars and Implications for Crustal Evolution. Geophysical Research Letters ***28,*** *4015-4018.*

Connerney, J.E. and others 1999. Magnetic Lineations in the Ancient Crust of Mars Science ***284,*** *794-798.*

Connerney, J.E. and others 2000. Response. Science ***287,*** *548.*

Curtis, S.A. and N.F. Ness 1988. Remanent Magnetism at Mars. Geophysical Research Letters ***15,*** *737-739.*

Harrison, C.G.A., 20002. Questions About Magnetic Lineations in the Ancient Crust of Mars, Science ***287,*** *547.*

*Helbig,K.,1963,Some integrals of magnetic anomalies and their relation to the parameters of the disturbing body,Z.Geophys.**29**,83-96*

*Hood, L.L. and A. Zakharian 2001. Mapping and modeling of magnetic anomalies in the northern polar region of Mars. Journal of Geophysical Research **106**, 14,601-14,619.*

Langel, R.A. and W.J. Hinze 1998. The Magnetic Field of the Earth's Lithosphere: The Satellite Perspective, Cambridge University Press, Cambridge.

*Leweling M. and T. Spohn 1997. Mars: a magnetic field due to thermoremanence? Planetary and Space Science **45**, 1389-1400.*

MacMillan,W.D. 1958. The Theory of the Potential.Dover,New York, 469p.

*Mayhew, M.A. 1986. Approximate paleomagnetic poles for some of the New England Seamounts. Earth and Planetary Science Letters **79**, 185-194.*

*Ness, N.F. and others 1999. MGS Magnetic Fields and Electron Reflectometer Investigation: Discovery of paleomagnetic Fields Due to Crustal Remanence. Advances in Space Research **23**, 1879-1886.*

*Ness, N.F. and others 2000. Effects of magnetic anomalies discovered at Mars on the structure of the Martian ionosphere and solar wind interaction as follows from radio occultation experiments. Journal of Geophysical Research **105**, 15991-16004.*

*Nimmo, F., 2000. Dike intrusion as a possible cause of linear Martian magnetic anomalies. Geology **28**, 391-394.*

*Parker, R.L., L. Shure and J.A. Hildenbrand 1987. The application of inverse theory to seamount magnetism. Reviews of Geophysics **25**, 17-40.*

*Plouff,D. 1976 Gravity and magnetic fields of polygonal prisms and application to magnetic terrain corrections. Geophysics **41**,727-741*

Purucker, M. and others 2000. An altitude-normalized magnetic map of Mars and its interpretation. Geophysical Research Letters **27**, *2449-2452.*

Taylor,P.T. and Frawley,J.J. 1987. Magsat anomaly data over the Kursk region,U.S.S.R. ,Phys. Earth Planet. Inter. **45**,*255-265*

Zatman, S. D. Stegman, D. Ravat, P. Taylor and J. Frawley 2001. Geodynamic constraints on the age of the Martian magnetic anomaly construction. EOS Transactions AGU **82 (20)**, *S127.*

Area #	*Lat Range*	*Lon Range*
1	50S-10N	75W-135W
2	50S-10N	180W-120W
3	50S-10N	90W-30W
4	50S-10N	30W-30E
5	50S-10N	30E-90E
6	50S-10N	90E-150E
7	30S-30N	30W-30E

Table 1

Test Area Limits

Area	*#*	*Lat (deg)*	*Lon (deg)*	*Depth (km)*	*Moment 10^{16} A-m^2*	*Dip (deg)*	*Dec (deg)*	*rms fit (nT)*	*Paleolat (deg)*	*Paleolon (deg)*
1	1	28.5S	107.7W	40	1.9	-30	57	3.9	36.3N	18.1W
2	2	8.6S	145.0W	40	2.7	-47.7	3.7	6.2	69.6N	25.6E
2	3	14.8S	166.0W	0	16 A/m	-67.7	170	12	24.0S	7.1E
2	4	32.1S	163.3W	0	23 A/m	-41	-81	23	19.4N	90.6E
3	5	4.8S	54.1W	40	2.21	-3.5	176.7	5.4	82.6S	99.3E
3	6	31.5S	48.8W	160	3.66	-3.2	-18.7	5	55.3N	83.3W
3	7	37.2S	65.2W	160	3.5	-14.9	12.5	4.5	58.3N	41.1W
7	8	4.7N	17.0W	20	1.46	-9.6	180	5.3	89.8S	163.4E
7	9	1.4N	0.9E	20	1.32	-9.6	172.3	5.6	81.6S	115.1E

Table 2
Dipole Models and paleo-poles

Figures:

1. Global maps for X (North), Y (East) and Z (Vertical) components.

2. Locations of seven sub-areas where isolated anomalies were located.

3. Samples of selected profiles of five adjacent MGS tracks, Total Field, X, Y and Z.

4. Example of track coverage for Area 2. Other areas display a similar high density of orbits.

5 a-c) Data points used for input to inverse procedure from anomaly 2. d) Rms Contours for anomaly 2.

6 a-g) Component contours for areas and dipole fit to the anomaly fields. Contour intervals vary and are given for each area.

7. Anomaly-paleo-pole positions, X represents location of the paleo-pole triangles indicate anomaly location.

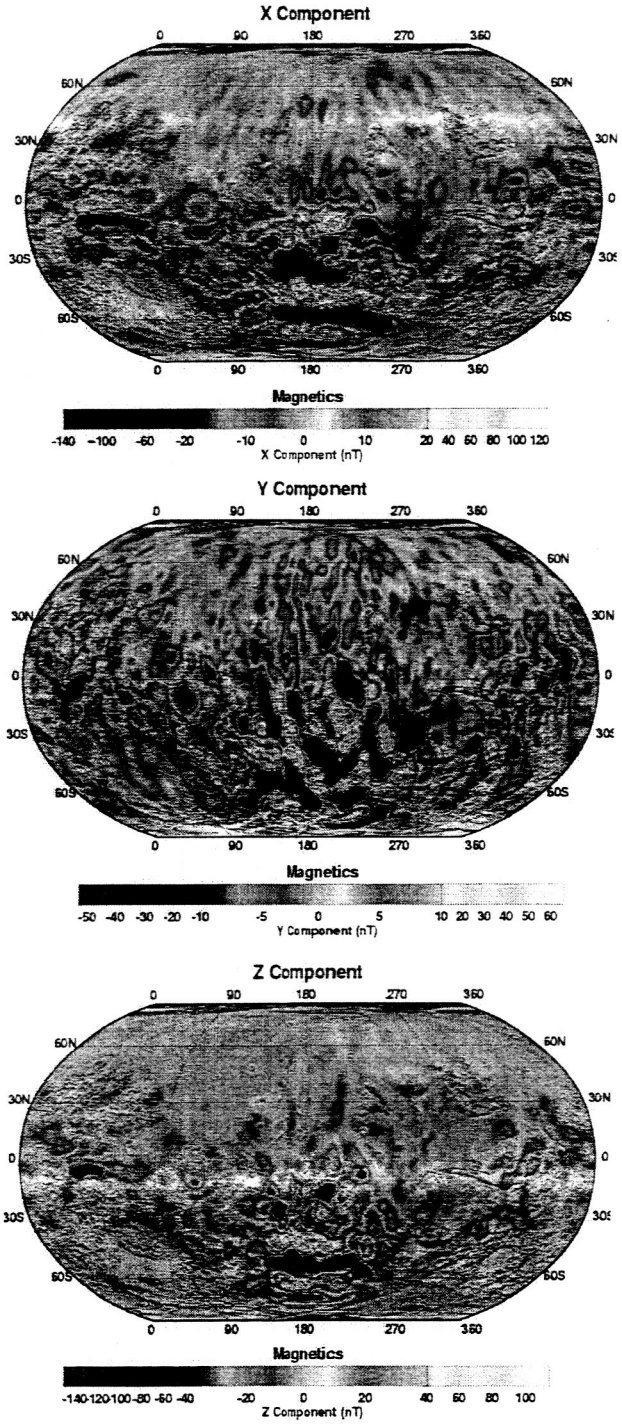
X Component
0
90
180
270
360
60N
30N
0
30S
60S
Magnetics
-140 -100 -60 -20 -10 0 10 20 40 60 80 100 120
X Component (nT)
Y Component
Magnetics
-50 -40 -30 -20 -10 -5 0 5 10 20 30 40 50 60
Y Component (nT)
Z Component
Magnetics
-140-120-100-80 -60 -40 -20 0 20 40 60 80 100
Z Component (nT)

Figure 1 Global m,aps for North(X),East(Y) and vertical(Z) Components

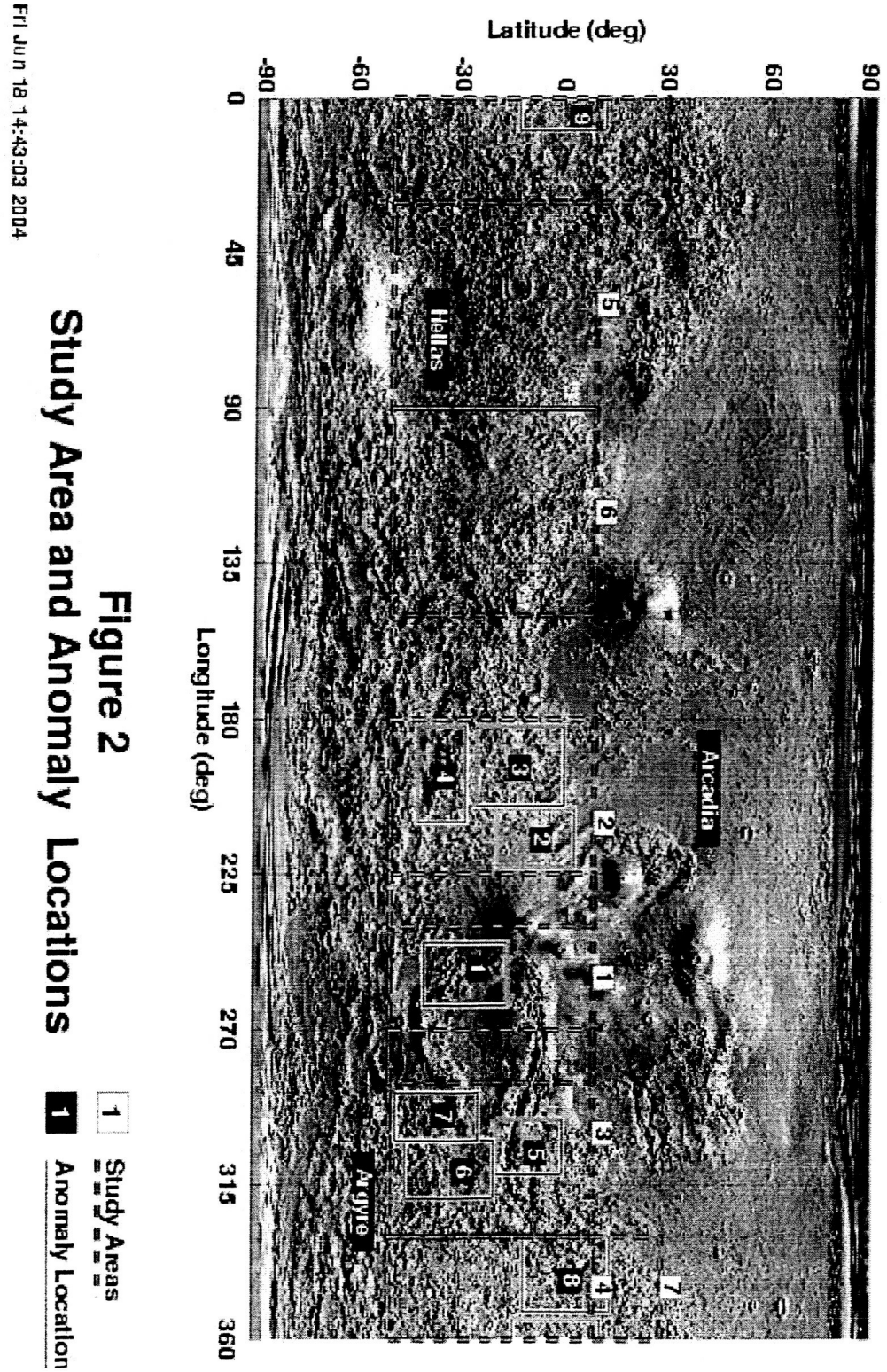

Figure 2 area locations

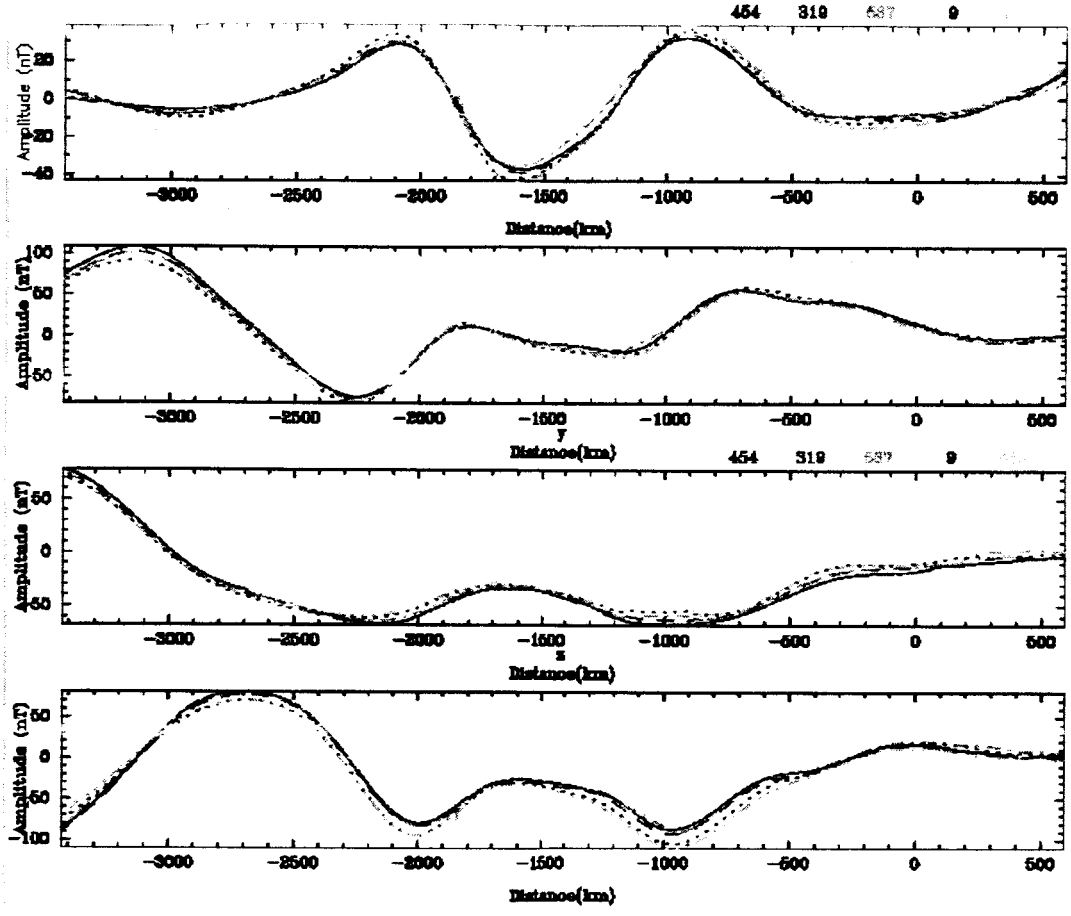

Figure 3 - Profiles of adjacent tracks

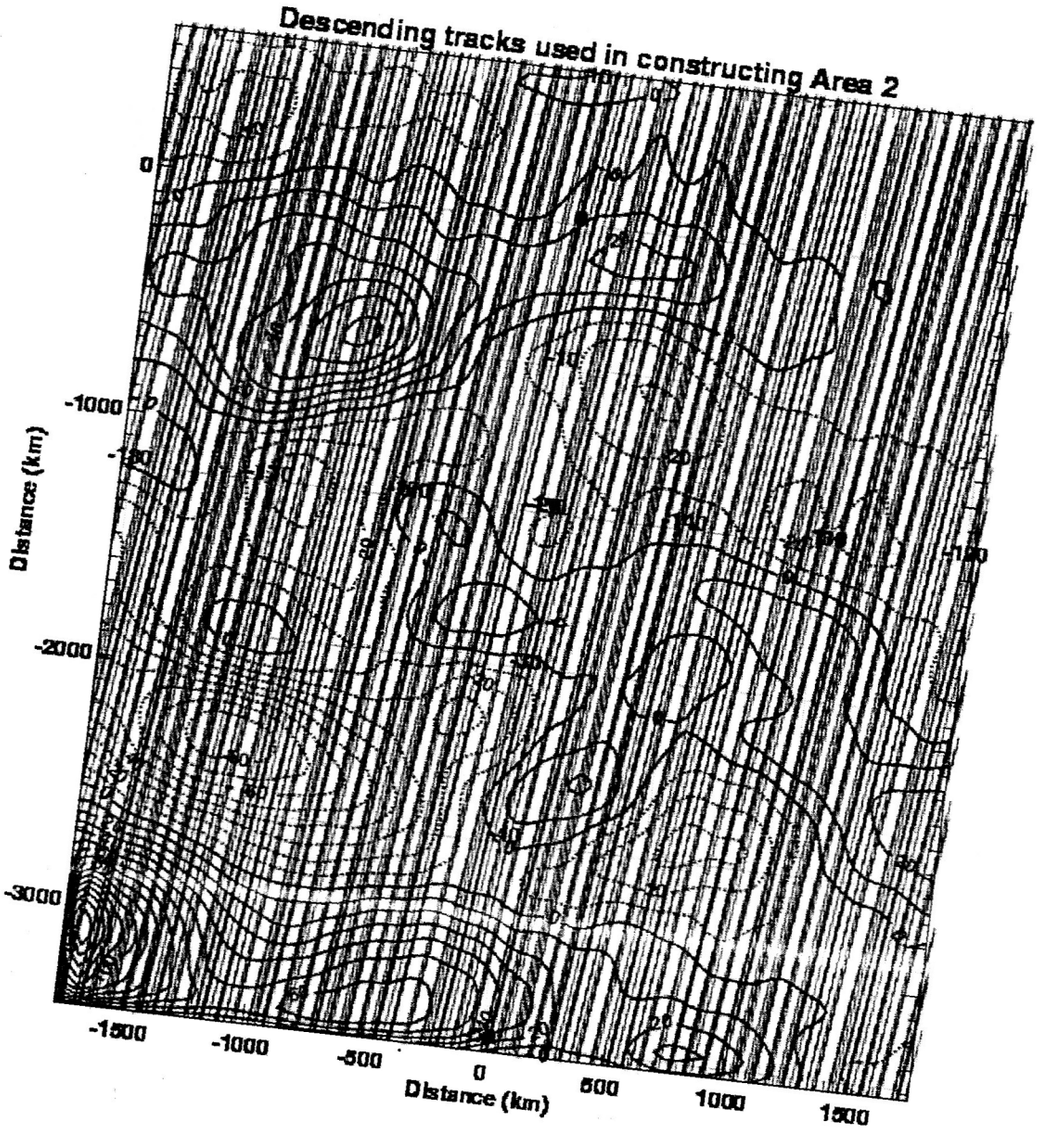

Figure 4 - X Component

Wed Feb 11 11:15:45 2004

Figure 4 - Tracks used in processing area 2

c.i.=10 nT

Figure 5

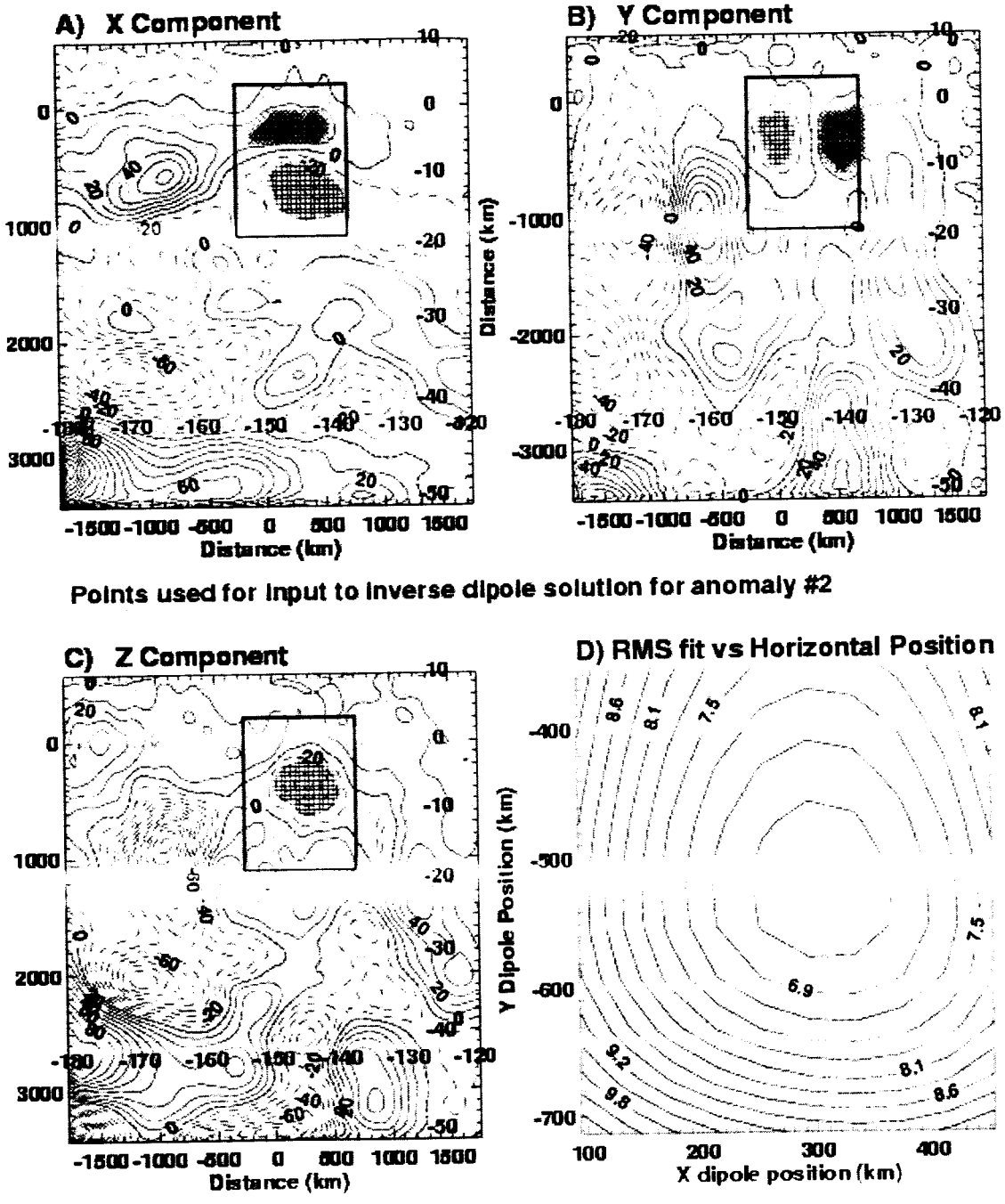

Fig5 Points used for input to inverse program for Area 2

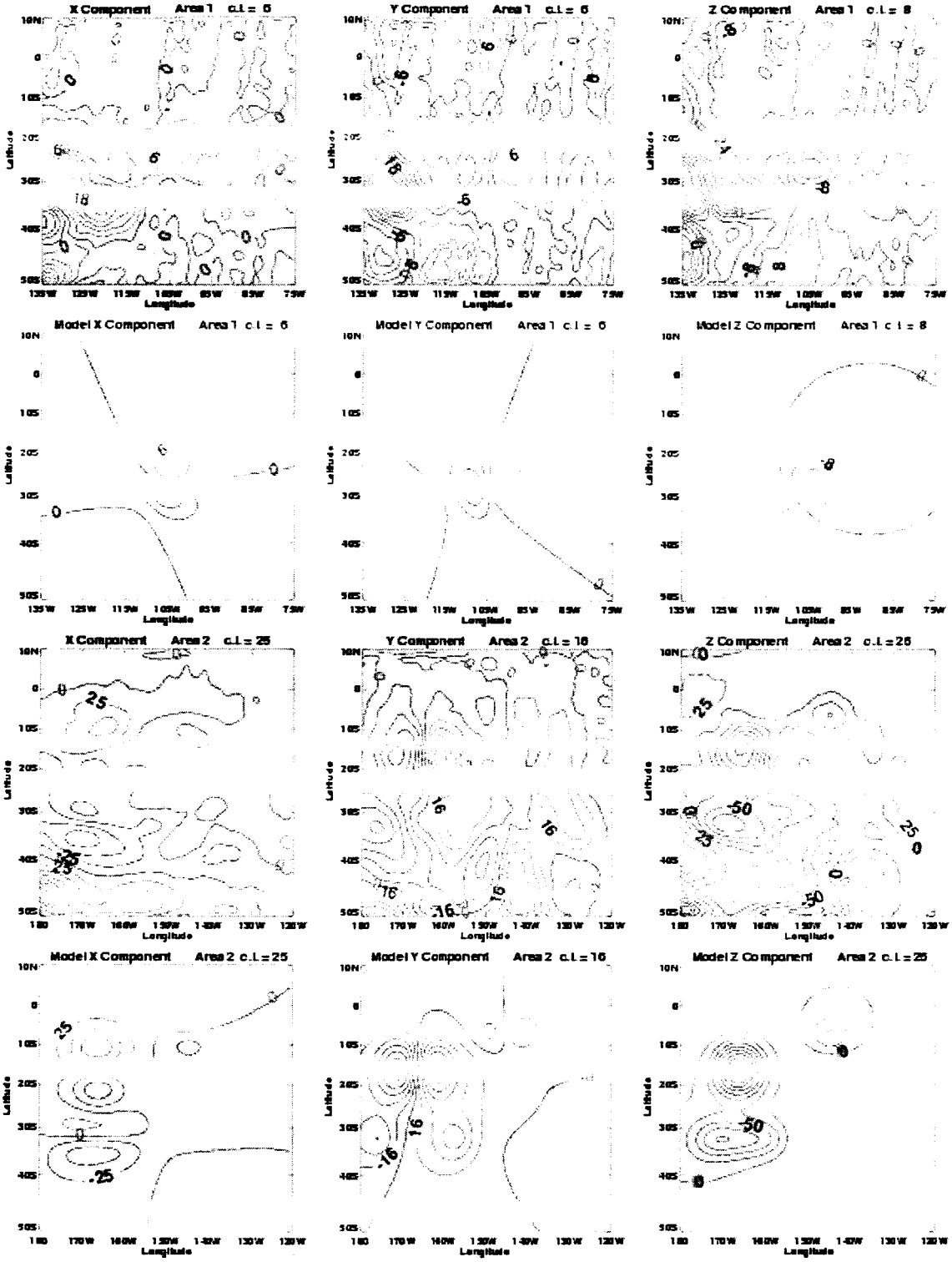

Figure 6a Crustal anomaly maps and dipole models.

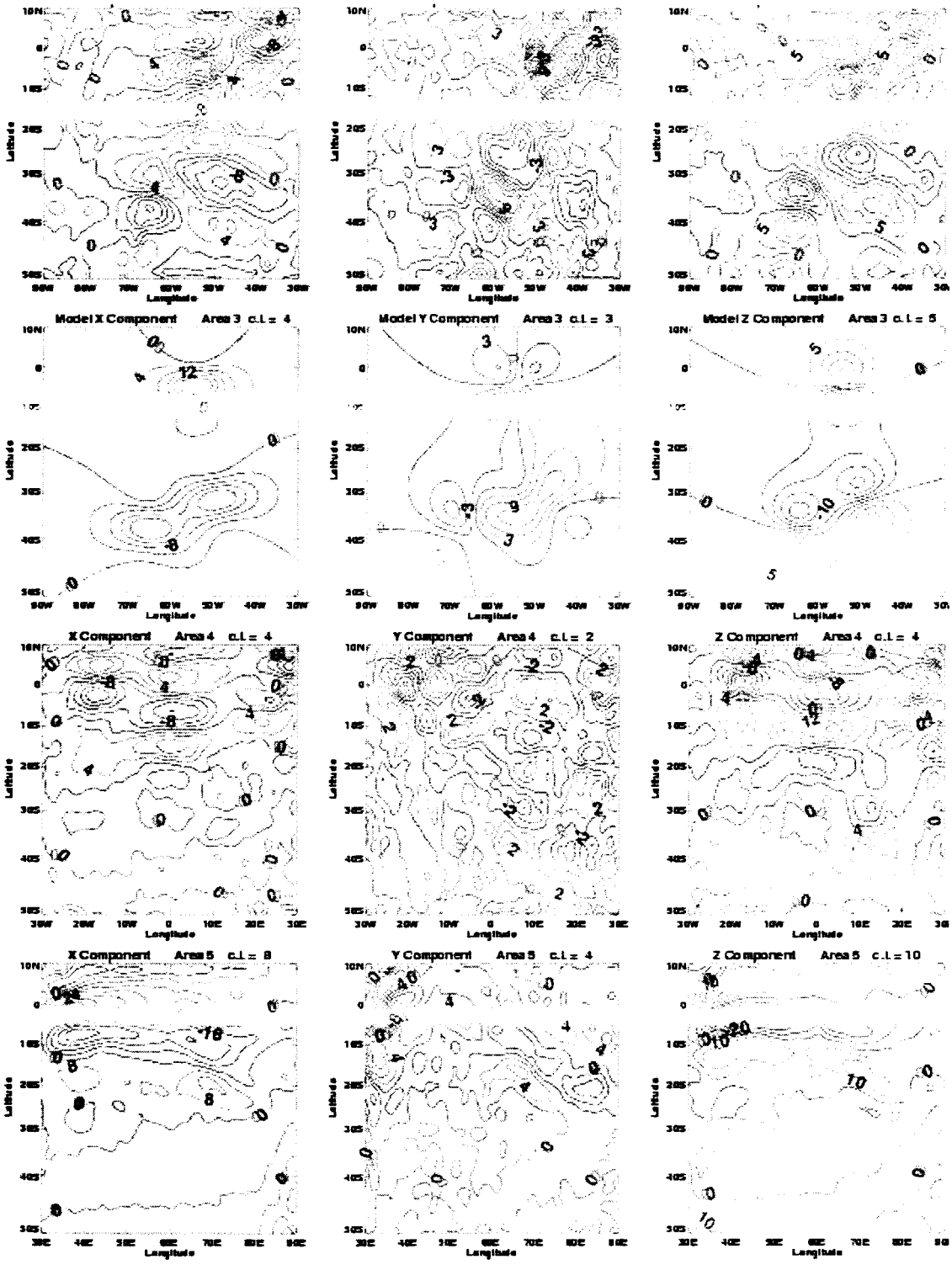

Figure 6b Crustal Anomaly maps and dipole models

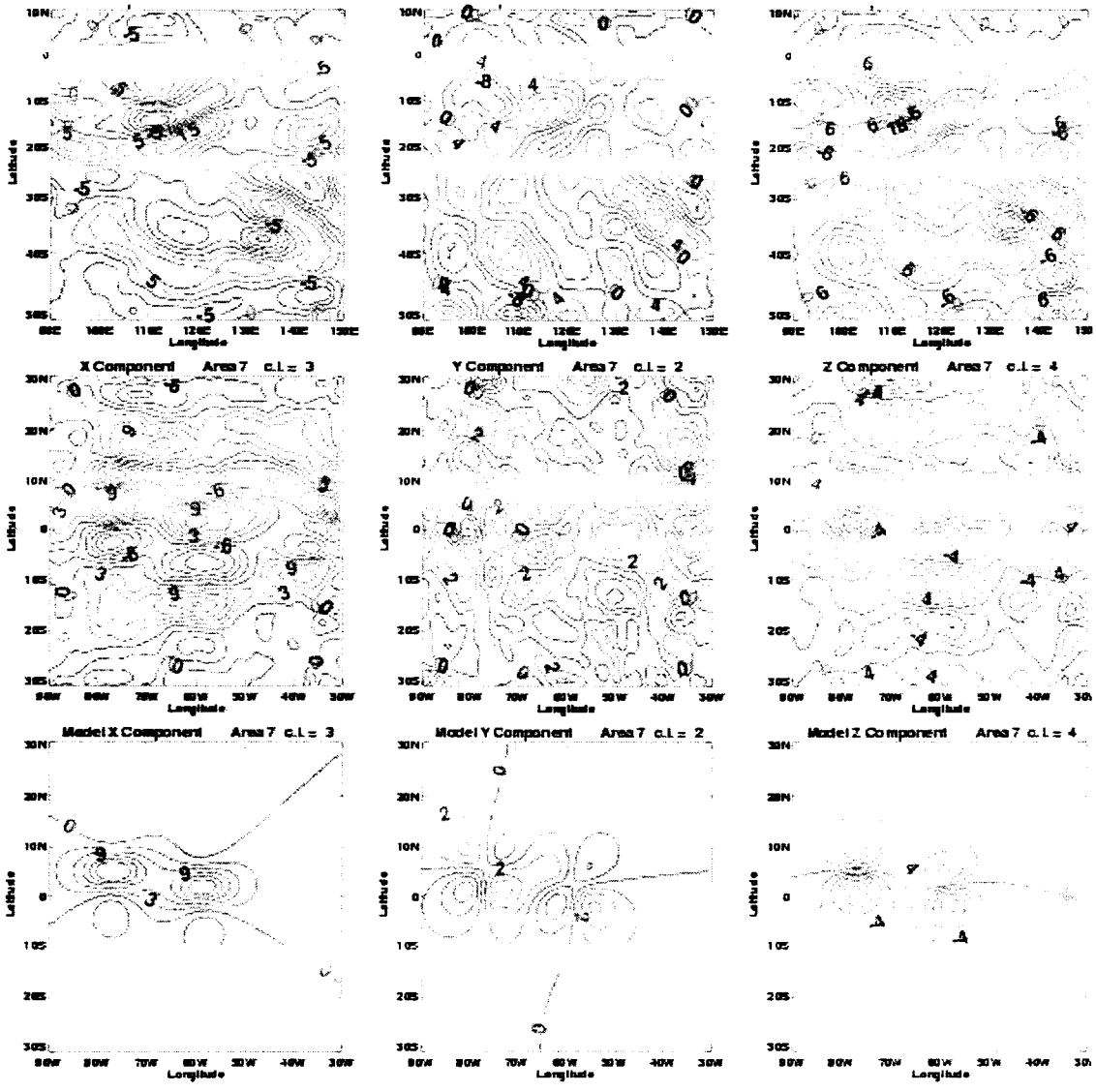

Figure 6

contours for areas 1-7

model field contours are shown below measured field

Mon Jun 28 10:14:41 2004

Figure 6c Crustal anomaly maps and dipoles

Anomaly and Paleopole locations on Topography

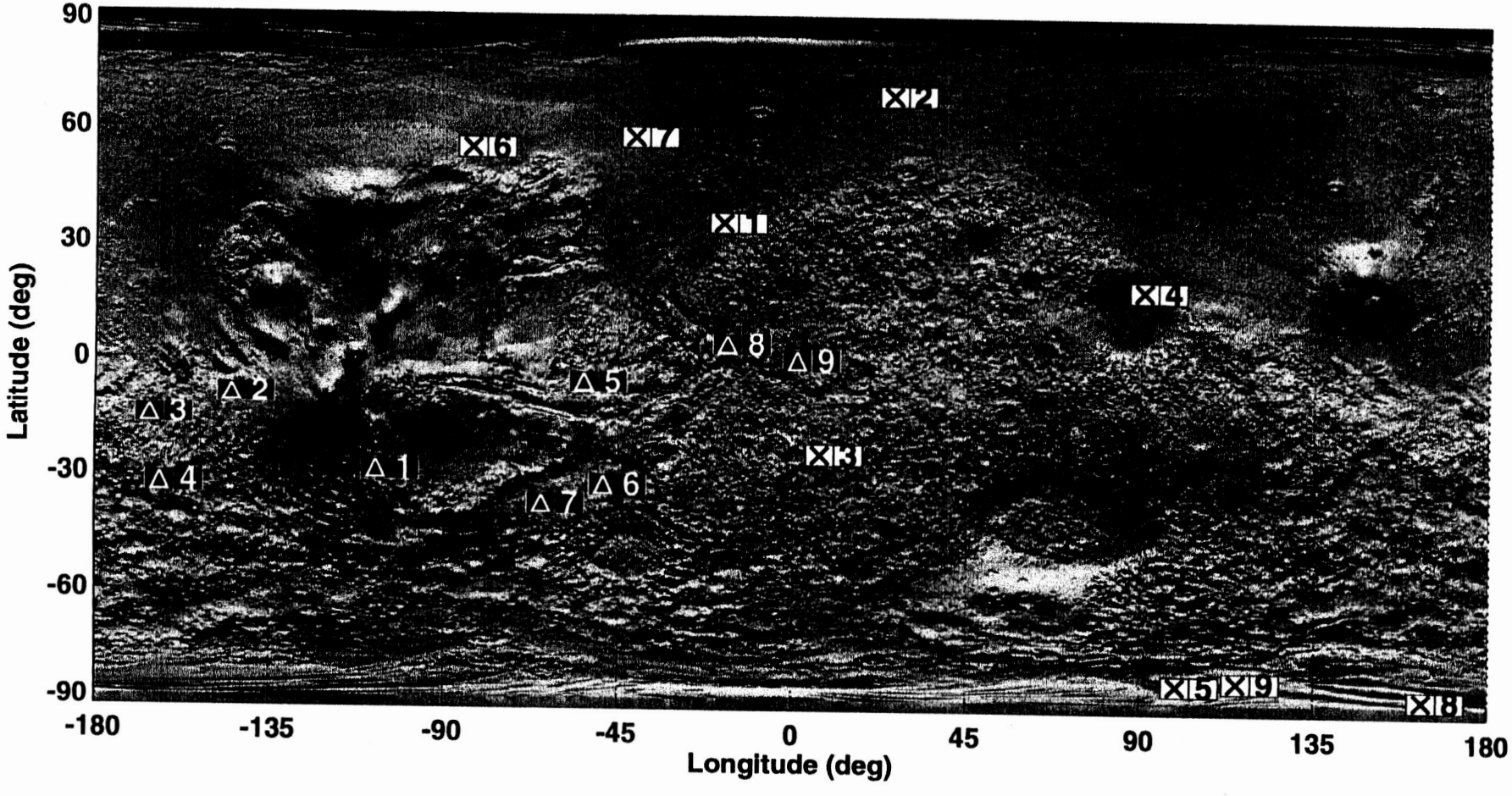

Figure 7

X Paleopoles

Δ Anomaly Locations

Tue Aug 10 07:50:07 2004

POPULAR SUMMARY

A Standard Atmosphere of the Antarctic Plateau

Ashwin Mahesh and Dan Lubin

Submitted to the *Journal of Climate*, August 2004

Climate models often rely on standard atmospheres to represent various regions because it is often computationally too difficult to include local representations from every location in the model. These standard profiles broadly capture the important physical and radiative characteristics of regional atmospheres, and become benchmarks for simulations by researchers. Such standards were made in the 1970s for most regions of the planet, but not for Antarctica. This is a significant omission, because Antarctica occupies a significant area (comparable to the United States) and is also very different from any place on Earth. The standard profiles of other regions made for use in climate models are not representative of Antarctica, and are therefore only of limited value as substitutes in climate models. This research is an effort fill the void in the scientific community's library of standard atmospheres, so that future representations of the region in climate models can be more accurate.

Using data from radiosondes, ozonesondes and satellite along with other observations from South Pole station, typical seasonal atmospheric profiles for the high plateau are compiled. Temperature profiles had to be corrected for measurement errors caused by the slow response of the recording thermistors. Proper representations of rapidly changing ozone concentrations (during the ozone hole) were also necessary, because the same total column amounts of ozone in the atmosphere correspond to